Field and Magic Angle Spinning frequency dependence of proton resonances in rotating solids

Kai Xue,[a] Riddhiman Sarkar,[b,c]* Zdeněk Tošner,[d] Bernd Reif [b,c] *

April 28, 2021

[a]Max Planck Institute for Biophysical Chemistry, Department of NMR Based Structural Biology, Am Fassberg. 11, Goettingen, Germany

[b] Helmholtz-Zentrum München (HMGU), Deutsches Forschungszentrum für Gesundheit und Umwelt, Ingolstädter Landstr. 1, 85764 Neuherberg, Germany

[c] Munich Center for Integrated Protein Science (CIPS-M) at Department Chemie, Technische Universität München (TUM), Lichtenbergstr. 4, 85747 Garching, Germany

[d] Department of chemistry, Faculty of Science, Charles University, Hlavova 8, 12842 Praha 2, Czech Republic

To whom correspondence should be addressed: reif@tum.de, riddhiman.sarkar@helmholtz-muenchen.de

Abstract

Proton detection in solid state NMR is continuously developing and allows one to gain new insights in structural biology. Overall, this progress is a result of the synergy between hardware development, new NMR methodology and new isotope labeling strategies, to name a few factors. Even though current developments are rapid, it is worthwhile to summarize what can currently be achieved employing proton detection in biological solids. We illustrate this by analysing the signal-to-noise ratio (SNR) for spectra obtained for a microcrystalline α-spectrin SH3 domain protein sample by (i) employing different degrees of chemical dilution to replace protons by incorporating deuterons in different sites, by (ii) variation of the magic angle spinning (MAS) frequencies between 20-110 kHz, and by (iii) variation of the static magnetic field B_0. The experimental SNR values are validated with numerical simulations employing up to 9 proton spins. Although in reality a protein would contain far more than 9 protons, in a deuterated environment this is a sufficient number to achieve satisfactory simulations consistent with the experimental data. The key results of this analysis are (i) with current hardware, deuteration is still necessary to record spectra of optimum quality; (ii) $^{13}CH_3$ isotopomers for methyl groups yield the best SNR when MAS frequencies above 100 kHz are available; and (iii) sensitivity increases with a factor beyond B0 3/2 with the static magnetic field due to a transition of proton-proton dipolar interactions from a strong to a weak coupling limit.

Introduction

Proton spins have the highest gyromagnetic ratio, and therefore the highest magnetic moment, among all stable isotopes across the periodic table, resulting in maximum sensitivity in NMR spectra. For the same reason, proton experience the strongest dipole-dipole interactions in solids. Unless averaged by fast tumbling in solution, dipolar fields cause a fast decay of transverse proton magnetization and induce broad lines, resulting in little information in the spectra. Dipolar interactions can be decoupled if solid samples are rotated at an angle of $\arctan[\sqrt{2}]$ with respect to the magnetic field[1, 2], under the assumption of sufficiently fast rotation. Unfortunately, sufficient rotation rates are not achievable and residual homogeneous interactions remain. Faster spinning leads to better averaging and yields narrower lines in proton NMR spectra. Although well-known, the advantages of proton detection were "rediscovered" in biological solids only 20 years ago [3, 4] [5-8] . Correlation spectra of unprecedented quality were obtained by means of chemical dilution of the proton dipolar coupling network. The reduction in sensitivity due to the replacement of protons with deuterons is compensated by the enhancement in resolution, with the result that signal-to-noise ratio (SNR) increases by a factor of $\left(\frac{\gamma_H}{\gamma_X}\right)^{\frac{3}{2}}$ due to proton detection, where γ_H and γ_X are the gyromagnetic ratios of proton and X nucleus, respectively. Despite the difficulties in expressing proteins in deuterated media, challenges in back protonation at exchangeable sites for a variety of systems, and the lack of weak long range proton contacts in highly deuterated samples, this strategy led to a revolution in biological solid-state NMR[9] [10].

Similarly, high-resolution spectra can be recorded for methyl protons in perdeuterated peptides and proteins. To achieve this, bacteria that over-express the protein are grown in a medium containing amino acid precursors such as pyruvate [11] or α-ketoisovalerate [12] that allow selective labeling of methyl groups in aliphatic side chains. Alternatively, randomly protonated (RAP) protein samples can be obtained by growing bacteria in a medium containing ^{2}H,^{13}C labeled glucose in the presence of varying amounts of H_2O (5-20 %) [13].

The strict requirement for a high degree of deuteration was able to be relaxed as faster spinning MAS probes became available. ^{1}H,^{15}N correlation spectra recorded at a MAS

frequency of 60 kHz[14] using samples that contain 100 % protons at exchangeable sites have similar quality to spectra that are obtained from 20 % back-exchanged samples at 20 kHz MAS[15, 16]. In 2016, the first structure of a fully protonated protein was determined employing a probe that achieved a MAS frequency of 110 kHz. Proton detection has become a popular tool [17-20] for investigating large biomolecules in recent years, and new strategies ranging from hardware development to isotope labelling have been developed. A wide variety of supramolecular assemblies[21, 22] such as amyloid fibrils [23-29], membrane proteins, ribosomal subunits[30] and viral capsids [31-33] have meanwhile been studied with atomic resolution employing proton-detected MAS solid state NMR.

Clearly, an MAS frequency of 110 kHz MAS is not sufficient to overcome the dipolar coupling network[34] among protons in the complete absence of chemical dilution. Therefore, the quest for higher MAS frequencies continues [35, 36]. However, increasing MAS frequency forces the use of smaller rotor volumes, translating into a smaller number of spins and reduced absolute sensitivity. Higher static magnetic fields increase the sensitivity of the experiment due to the increased population differences between the nuclear spin states and detection of a higher frequency NMR signal. In addition, frequency differences between resonances increase with higher B_0 fields, which in turn weakens the effect of dipolar coupling among protons. Therefore, it is cumbersome to quantify and compare effects such as variations in sensitivity of spectra recorded using spectrometers that operate at different fields or that are equipped with probes using different rotor sizes.

The aim of this review is to highlight what can currently be achieved by solid-state NMR employing commercially available resources such as optimal hardware, isotope labelling schemes and methodology, and to discuss limitations that could be addressed in the future.

Andreas et al. acquired high resolution proton spectra of a fully protonated microcrystalline GB1 protein sample [37]. The experiments were performed at a B_0 field of 23.5 T, corresponding to a ^{1}H Larmor frequency of 1 GHz, employing an MAS frequency of 100 kHz. The data were subsequently used to calculate two protein structures *de novo* with high precision. However, at a B_0 field of 500 MHz, and employing the same MAS frequencies, a poor spectrum for a fully protonated SH3

domain sample is obtained[38]. We address here the question of which isotope labelling strategy, MAS frequency and B_0 field should be employed to yield spectra of optimum quality for biomolecules.

Sensitivity of a proton detected experiment

Following the notation of Ishii and Tycko[39], the signal-to-noise ratio (SNR) [40, 41] for unit time of a proton-detected ^{1}H-X (where X can be ^{15}N or ^{13}C) HSQC-like correlation experiment [42] can be described as:

$$\left(\frac{S}{N}\right)_{HSQC} = \frac{(<S(t_1,t_2)w(t_1,t_2)>)(Rt_2^{max})^{\frac{1}{2}}}{2^{\frac{1}{2}}<w(t_1,t_2)^2>^{\frac{1}{2}}}\left(\frac{A_H}{\rho_H}\right) \qquad \text{Eq. [1]}$$

Here $S(t_1, t_2)$ is a non-negative envelope function, $w(t_1, t_2)$ is an apodization window function, which in the case of a matched filter becomes equal to $S(t_1, t_2)$. R is the repetition rate of the experiments, and t_2^{max} is the length of the acquired time domain signal. $<x(t_1,t_2)>$ denotes the time average of x over time intervals [0, t_1^{max}] and [0, t_2^{max}].The $(\frac{A_H}{\rho_H})$ term contains various hardware- and sample-dependent factors and can be defined as:

$$\frac{A_H}{\rho_H} = \left(\frac{\pi\omega_H V Q_H}{kT}\right)^{1/2}\eta M_H \qquad \text{Eq. [2]}$$

where $\omega_H = -\gamma_H B_0$ is the Larmor frequency of protons. η, V, and Q_H are the filling factor, volume and quality factor of the RF coil [43] for proton detection, respectively, and T is an effective temperature for the total noise arising from the different hardware components, which is dependent on several factors such as the temperature of the detection coil and noise temperature of the preamplifier. For an HSQC-like experiment, $M_H = \frac{f^2\gamma_H^2\hbar^2 B_0 N_x}{4kT}$, where f denotes the (assumed identical) magnetization transfer efficiencies from ^{1}H-X before evolution in the indirect domain (t_1) and X-^{1}H before signal detection (t_2). N_x denotes the number density of X spins. Assuming that $\langle S(t_1,t_2)\rangle = \langle S(t_1)\rangle\langle S(t_2)\rangle$, $\langle w(t_1,t_2)\rangle = \langle w(t_1)\rangle\langle w(t_2)\rangle$ and that the window functions represent matched filters in both dimensions, the relative sensitivity of two HSQC experiments can be expressed as:

$$\frac{SNR_{s1}}{SNR_{s2}} = \left(\frac{W_{H,s2}}{W_{H,s1}}\right)^{\frac{1}{2}}\left(\frac{B_{0,s1}}{B_{0,s2}}\right)^{\frac{3}{2}}\left(\frac{f_{s1}}{f_{s2}}\right)^2\left(\frac{\langle S(t_1)\rangle_{s1}^2}{\langle S(t_1)\rangle_{s2}^2}\right)^{\frac{1}{2}}\left(\frac{R_{s1}\eta_{s1}(V_{s1}.Q_{H,s1})^{\frac{1}{2}}}{R_{s2}\eta_{s2}(V_{s2}.Q_{H,s2})^{\frac{1}{2}}}\left(\frac{T_{s2}}{T_{s1}}\right)^{\frac{3}{2}}\right) \qquad \text{Eq. [3]}$$

Here X_{s1}, X_{s2} denote the sets of parameters employed in experiments s_1 and s_2, respectively, and $W_H = (2\pi t_2^{max}\langle S(t_2)\rangle^2)^{-1}$ is analogous to the proton linewidths,

assuming Lorentzian lineshapes. It is convenient to include linewidth instead of the shape envelope function in the indirect dimension in [Eq. 3] too:

$$\frac{SNR_{S1}}{SNR_{S2}} = \left(\frac{W_{H,S2}}{W_{H,S1}}\right)^{\frac{1}{2}} \left(\frac{W_{X,S2}}{W_{X,S1}}\right)^{\frac{1}{2}} \left(\frac{t_{X,S1}^{max}}{t_{X,S2}^{max}}\right)^{\frac{1}{2}} \left(\frac{B_{0,S1}}{B_{0,S2}}\right)^{\frac{3}{2}} \left(\frac{f_{S1}}{f_{S2}}\right)^{2} \left(\frac{R_{S1}}{R_{S2}}\right) \left(\frac{\eta_{S1}(V_{S1}.Q_{H,S1})^{\frac{1}{2}}}{\eta_{S2}(V_{S2}.Q_{H,S2})^{\frac{1}{2}}} \left(\frac{T_{S2}}{T_{S1}}\right)^{\frac{3}{2}}\right) \quad \text{Eq. [4]}$$

where t_X^{max} and W_X can be estimated from an X- (^{15}N or ^{13}C in this review) detected 1D spectrum for resolved resonances. The last term in [Eq. 4] is dependent on hardware. This makes it challenging to compare the SNR for experiments recorded employing different spectrometers.

In solution-state NMR, 0.1% ethylbenzene in $CDCl_3$ is employed as a SNR standard [44]. For solid-state NMR, nothing similar has been widely adapted. Bryce and co-workers have suggested glycine, adamantane or polydimethylsilane as a sensitivity standard in the solid state[45] [46]. More recently, endohedral fullerenes such as H_2@C60 have been proposed[47]. There, ortho H_2 molecules can be incorporated with ~ 100% yield inside stable fullerene cages. The proton spin density is thus well characterized [48, 49]. As the partially averaged dipolar coupling between the two protons is typically less than 1 kHz [47], it is possible to average out the remaining dipolar coupling with relatively slow MAS (< 10 kHz). The proton chemical shift of -7.25 ppm can also be used as a secondary or primary chemical shift reference for ^{13}C or ^{1}H respectively. Solid sensitivity standards have the disadvantage that the error bar associated with the variable amount of material packed into the rotor is comparatively large. Small molecules in solution would in principle be better suited to quantifying the SNR for solid-state NMR. The volume of a rotor is well defined, and the concentration of a solution is easily quantified. Furthermore, the sensitivity is not affected by insufficient decoupling or magic angle misadjustment. Tight sealing of the rotor is, however, an issue. It has been shown for protein complexes in solution [50, 51] that this problem can be overcome. We suggest to use a 5 mM glucose solution in D_2O as a standard to determine the **absolute** sensitivity of a ^{1}H detected experiment for a MAS probe. To quantify the **relative** sensitivity with respect to a single pulse reference experiment, we employ a ^{2}H,^{13}C,^{15}N labeled fMLF sample which is commercially available. This allows indirect specification of the decoupling performance, the magic angle setting, the rf homogeneity of the probe and the transfer efficiencies of a particular triple resonance experiment [52-57] [58].

Factors affecting proton linewidth

The proton linewidth is determined by both homogeneous and inhomogeneous contributions. The homogeneous part arises from both coherent and incoherent effects. The homonuclear dipolar Hamiltonian is a homogeneous interaction in the sense of Maricq and Waugh and does not commute with itself at different times [59] for more than a pair of protons. As a consequence, proton coherences dephase quickly in a spin echo experiment. Faster sample spinning reduces this coherent homogeneous contribution to the linewidth by yielding more efficient averaging of ^{1}H, ^{1}H dipolar interactions. The incoherent effects are due to relaxation.

In the solid state, homogeneous contributions originating from the strong proton dipolar coupling network typically determine the proton linewidth. Contributions to the inhomogeneous linewidth arise from B_0 inhomogeneity and the anisotropy of bulk magnetic susceptibility (ABMS) [60, 61]. ABMS yields slightly different chemical shifts for the same chemical site in different crystallites in a powdered sample. The contribution from ABMS cannot be completely averaged by MAS. In fortunate cases, an ABMS contribution of ~ 0.2 ppm [62] in the proton spectrum of a crystalline protein can be expected [63], which is less than the homogeneous linewidth. In solution, contributions originating from sample heterogeneity, anisotropy of the bulk magnetic susceptibility and instrumental instabilities are typically negligible compared to the homogeneous contributions from relaxation.

Due to the homogeneous nature of the dipolar Hamiltonian, the description of the proton environment in a real sample is challenging. A given proton experiences many internuclear interactions of different magnitudes. The contribution to linewidth depends on the relative orientation of the dipolar coupling tensors with respect to one another. Zorin *et. al* [64] [65, 66] have introduced the concept of an effective dipolar coupling

$$d^{RSS,j} = \left(\frac{\mu_0 \gamma_H^2 \hbar}{4\pi}\right) \sqrt{\sum_{k \neq j} \left(\frac{1}{r_{j,k}^3}\right)^2} \qquad \text{Eq. [5]}$$

where d^{RSS} refers to the root mean square of the dipolar couplings of a particular proton j to all neighboring protons. Hodgkinson *et al* have included the effect of the orientations of the coupling tensors in the description of the linewidth [62].

It is not practical to describe the many different proton environments in a protein sample using a single descriptor d^{RSS}. A couple of theoretical approaches have been introduced to evaluate the quality of proton detected NMR spectra under MAS: (i) Extensive numerical simulations employing increasing computational power and advancements in calculation methods, and (ii) calculation of second moments of proton spectra.

Estimation of the proton line width using SPINACH simulations involving up to 48 protons

One bottleneck in exact numerical simulations of proton lines in the solid state is the computational power needed for large spin ensembles. Recently, the Fokker-Planck formalism [67] has been applied to calculate ^{1}H spectra of the β-L-Asp-L-Ala dipeptide as a function of MAS frequency in the range 15-120 kHz. In the simulations, 48 protons [68] were accounted, for representing one unit cell, and periodic boundary conditions were assumed to generate relevant proton-proton dipolar interactions within the spin system. Application of state space restrictions, where all multi-spin components involving more than 3 spins are ignored, allowed the problem to fit into the memory of a high-performance supercomputer (12 processors) resulting in a calculation wall-time of 6-10 days per single proton spectrum. As relaxation was ignored in the simulation, only the homogeneous part of the apparent transverse relaxation time constant (T_2') coming from dipolar interactions could be extracted.

The site-specific proton transverse relaxation time T_2' was measured in spin echo experiments at a B_0 field of 850 MHz for MAS frequencies in the range of 30 kHz to 100 kHz and correlates well with the simulations [68]. The variation of ^{1}H T_2' with MAS frequency was fitted using a linear-quadratic model. Isolated spin pairs exhibiting a strong dipolar interaction with large chemical shift differences yield a $\frac{1}{\omega_r^2}$ dependence (where ω_r is the MAS frequency expressed in rad s^{-1}). On the other hand, isolated protons show a $\frac{1}{\omega_r}$ dependence. In addition, rigid CH_2 groups in small organic compounds that have a large ABMS show a decrease in line width by a factor of 2 when the MAS frequency is increased from 100 to 141 kHz.

Estimate of the proton line width via the second moment approach

Recently, the proton line width under MAS was estimated [69] using the semi-analytical method of second-moment calculations assuming a Gaussian lineshape, following the approach introduced by van Vleck [70]. The second moment does not require knowledge of matrix elements of Hamiltonians as it only depends on the traces of the dipolar coupling tensors. The calculation of the second moment is therefore computationally economical. Whereas a 12-spin simulation employing the Liouville von Neumann equation requires ~ 17-18 hours using 12 processors, the second moment calculation can be performed in ~ 20 minutes for a spin system with 200-250 spins. The simulated linewidths agree very well with the experimental linewidth in deuterated 100% back-exchanged ubiquitin, while the agreement is worse in the fully protonated protein. However, only information about linewidths is available from this approach and therefore important details about spin dynamics cannot be obtained.

Estimate of the proton linewidths of methyl groups via 9-spin SIMPSON simulations in a deuterated environment

The central questions that we address here are (i) how does the SNR for proton detection vary as a function of the MAS frequency and the external B_0 field for a model protein, and (ii) which isotope labelling scheme yields the optimal SNR for a given set of experimental conditions?

We focus here on $^{1}H,^{13}C$ correlation experiments on the methyl groups. Methyl groups are important reporters of structure [71-73] as they mostly appear in the hydrophobic core region of a protein. Methyl groups have little chemical shift dispersion and have the highest proton density of all functional groups in a protein. Therefore, inter- and intra-methyl dipolar couplings are the most difficult to average out by MAS. Figure 1 shows a residue-specific comparison of the d^{RSS} values for methyl and backbone amide protons of the α-spectrin SH3 domain. High d^{RSS} values result in short T_2' relaxation times and therefore larger proton linewidths. This was also observed in the pioneering work of Andreas *et al.* [74].

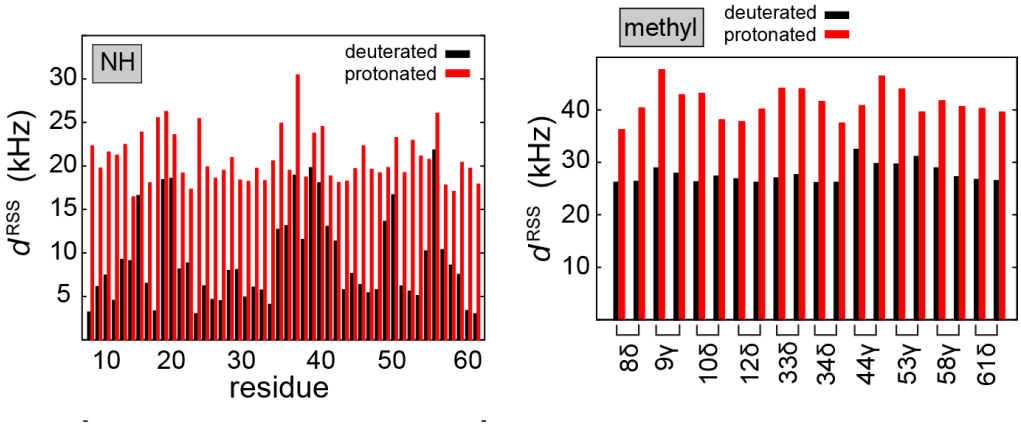

Figure 1. *$^{1}H, ^{1}H$ effective dipolar couplings d^{RSS} for amide and methyl protons in α-spectrin SH3 (PDB ID: 2NUZ) for protonated (red) and deuterated (black) samples. d^{RSS} was calculated considering all protons within a radius of 10 Å. Adapted with permission from ref 38, Nature Publishing Group.*

The methyl proton density can be varied by selectively incorporating the isotopomers $^{13}CHD_2$, $^{13}CH_2D$ and $^{13}CH_3$ in valine and leucine residues, while the rest of the protein is perdeuterated. It is ideally possible to apply similar strategies to label other amino acids containing methyl groups. However, this has not been discussed in this review.

These experimental spectra were then used to validate numerical simulations, which were then themselves used to predict the maximum achievable SNR for a particular set of experimental parameters such as MAS frequency, B_0 field and methyl isotopomer employed.

Figure 2A shows $^{1}H,^{13}C$ correlation spectra for fully protonated and partially deuterated samples of α-spectrin SH3 domain recorded at 500 MHz and 106 kHz MAS. The deuterated sample was selectively $^{13}CH_3$ methyl protonated at valine and leucine sites. Several cross peaks in the fully protonated sample, those originating from V53γ1, V9γ1 and V23γ1, are broadened beyond detection. In addition, the cross-peak intensities in the $^{13}CH_3$ sample vary significantly, by almost one order of magnitude. If the dipolar couplings amongst protons were fully averaged out by rapid tumbling or MAS, one would expect the cross-peak intensities to be equal. The mean SNR in the selectively $^{13}CH_3$ labelled sample is ~ 2.2 times (Figure 2D) higher than that for the fully protonated sample, while the ratios of the average ^{1}H and ^{13}C linewidths in the protonated and $^{13}CH_3$ labelled samples are ~ 2.9:1 and ~ 2.4:1, respectively (Figures 2C and E). Although *de novo* structure determination from fully protonated samples is possible for

favorable cases [74, 75], it is clear that spectra recorded with MAS frequencies of the order of 100 kHz are still broadened by proton-proton dipolar interactions and can be improved by deuteration.

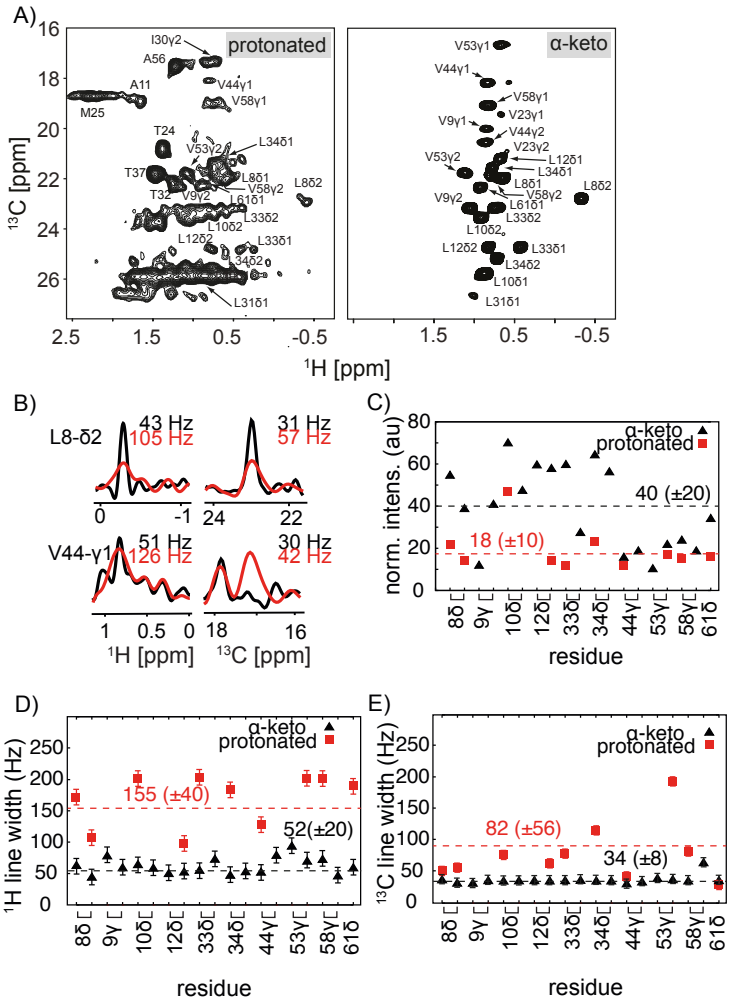

Figure 2. *Comparison of methyl spectral properties for protonated and selectively protonated microcrystalline SH3. Selective methyl labelling was achieved using α–ketoisovalerate in the bacterial growth medium [76]. A) ^{1}H,^{13}C correlation spectra for protonated SH3 (left) and methyl protonated SH3 (right). B) 1D traces along the ^{1}H and the ^{13}C dimension for protonated (red) and LV labelled SH3 (black) for selected residues. C) Methyl cross peak intensities for a protonated and LV labelled SH3 D) Proton line width of for protonated and α–keto labelled SH3. E) Carbon line width of for protonated and LV labelled SH3. All experiments were recorded at a magnetic field strength of 11.75 T, corresponding to a ^{1}H Larmor frequency of 500 MHz. The MAS rotation frequency was set to 106 kHz. Figure adapted with permission from ref 38, Nature Publishing Group.*

Numerical simulations using SIMPSON [77, 78] were employed to get a better understanding of the lineshapes and intensities of cross peaks as functions of the MAS

frequency, B_0 field or the chemical shift difference of methyl groups, and the proton density. As a result of recent developments in SIMPSON, it is possible to implement simulations in Hilbert space without any approximations to the spin dynamics for up to 10-12 spins [78]. First, we consider the proton spectrum of a single $^{13}CH_3$ group. The three protons of a methyl group are chemically equivalent, but magnetically inequivalent due to the different orientations of the dipolar coupling tensors.

Due to methyl group rotation, the dipolar couplings among protons are scaled by a factor of $\frac{1}{2}[3\cos^2\theta-1]=-1/2$ for $\theta = 90.0°$, where θ is the angle between C-H dipolar coupling and the the methyl rotation axis (along the C-C bond). The resulting effective dipolar coupling is on the order of ~ -10.5 kHz. In the static case, the spectrum for an isolated methyl group is relatively narrow thanks to the intense central line (Figure 3A). By contrast, the spectrum is broadened beyond detection for two mutually coupled methyl groups (Figure 4A). Under MAS, the proton spectrum for a single methyl group simplifies further and the center band intensity approaches its maximum at around a MAS frequency of employed 40 kHz as seen in Figure 3C.

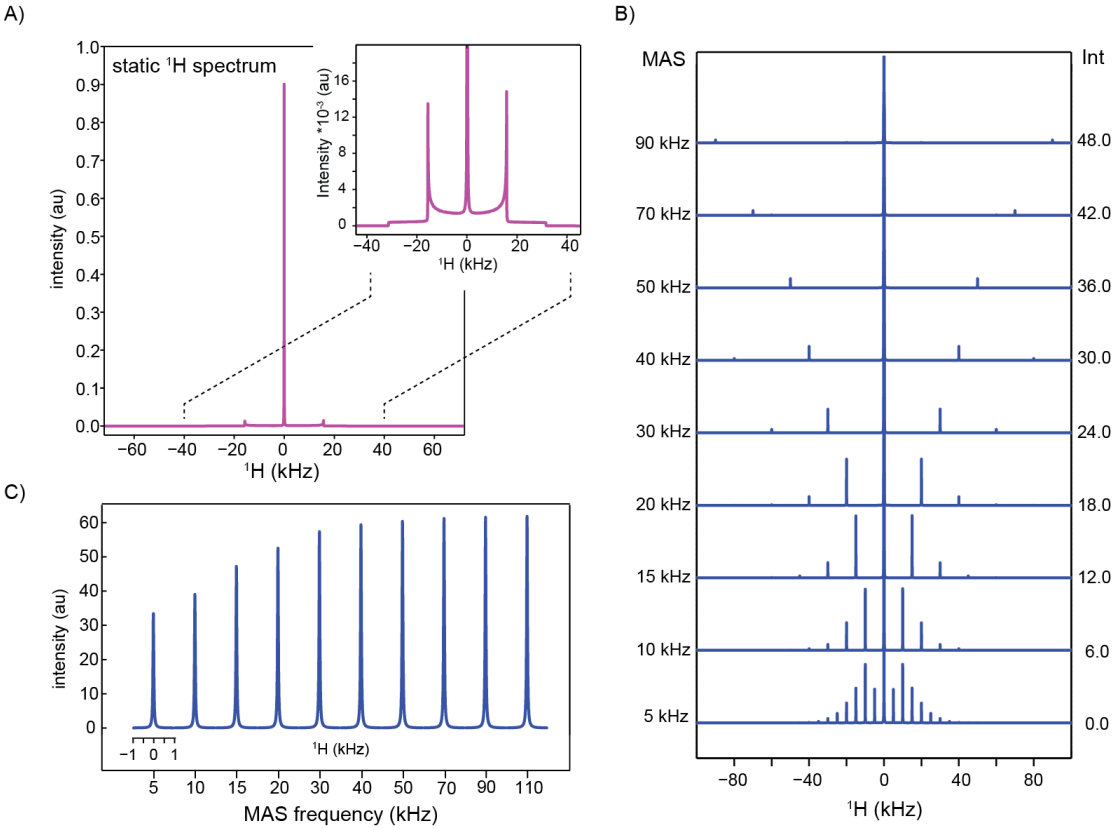

Figure 3. *¹H spectra simulated for an isolated methyl group. A) Static methyl proton spectrum featuring a sharp centre peak with dipolar Pake pattern at the baseline (inset) B) ¹H spectra*

under MAS of an isolated methyl group. C) MAS rate dependent ^{1}H centre band intensities. In all subspectra, a spectral window of 2 kHz is shown. Figure adapted with permission from ref 81, ACS.

For a methyl group interacting with a second methyl group, a MAS frequency of more than 110 kHz is necessary to yield maximum intensity (Figure 4C). For interacting methyl groups, the proton spectrum varies depending on the relative orientation, chemical shift difference and distance between the two methyl groups. The dependence of the intensity of the proton spectrum on the relative orientation of their dipolar coupling tensors for a pair of methyl groups is shown in Figure 5. Consideration of d^{RSS} fails to take all these factors into account. Assuming an orientation of the 2 methyl groups similar to that shown in Figure 5C, a ^{1}H chemical shift difference of 200 Hz and a dipolar coupling of 2 kHz, the MAS dependence of the calculated intensities of the proton lines (shown for one of the two methyls) is as shown in Figure 4B,C. The broad feature observed in the static spectrum averages out as a function of the MAS frequency. From the comparison of the proton spectra calculated for a single methyl group and a pair (Figure 6), it is clear that a MAS frequency of 70 kHz is sufficient to eliminate the broad feature at the base of the center band, whereas at a MAS frequency of 5 kHz, the broadening is significant. At 110 kHz MAS, the peak intensity of the center band approaches its maximum without notable changes in the proton linewidth.

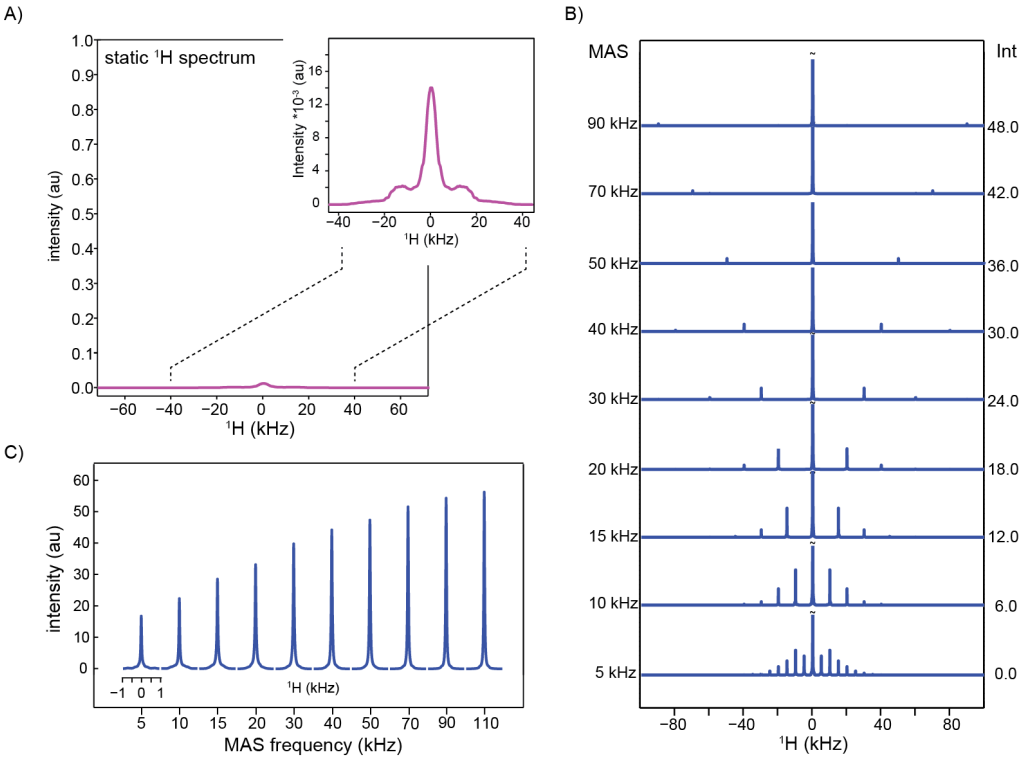

Figure 4. *¹H lineshapes simulated for a methyl group interacting with a second methyl. Methyl-methyl interactions introduce a homogeneous Hamiltonian in the sense of Maricq and Waugh [79]. In the simulation, a chemical shift difference of 200 Hz, an inter-methyl proton-proton dipolar coupling constant of 2000 Hz, and the perpendicular orientation of the effective C-H vectors (as shown in Figure 5C) have been assumed. Qualitatively similar behavior is obtained for other orientations. A) The static proton spectrum is very broad with significant intensity over a range of 40 kHz. B) Under MAS, the intensity of the powder pattern is distributesdinto a spinning sideband manifold, with more intensity accumulating in the centre band at faster spinning. C) ¹H methyl spectra at different MAS frequencies, focusing on the centre band. Figure adapted with permission from ref 81, ACS.*

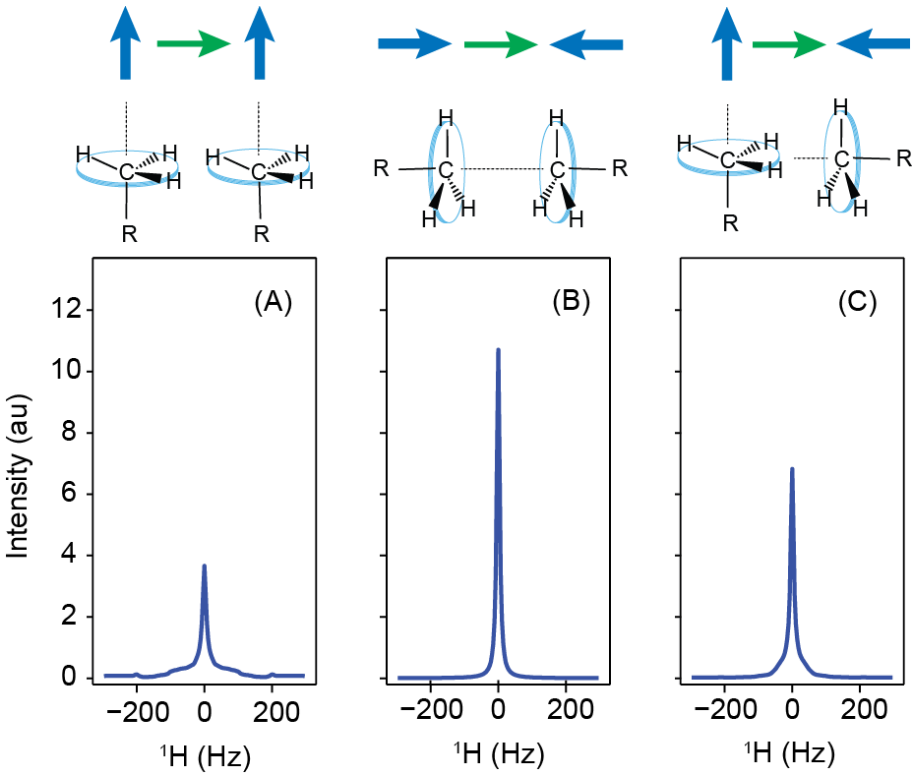

Figure 5. *Dependence of the ^{1}H lineshape on the methyl-methyl orientation. Spectra are simulated for different geometrical configurations. In the simulation, 3 explicit protons for each methyl group (6 spins in total) are assumed. A MAS frequency of 50 kHz, a chemical shift difference of 200 Hz and an inter-methyl proton-proton dipolar coupling constant of 2 kHz are assumed. Spectral changes arise due to different arrangements of the intra- and inter-methyl dipolar coupling tensors, depicted with blue and green vectors for intra- and inter-methyl interactions, respectively. Figure adapted with permission from ref 81, ACS.*

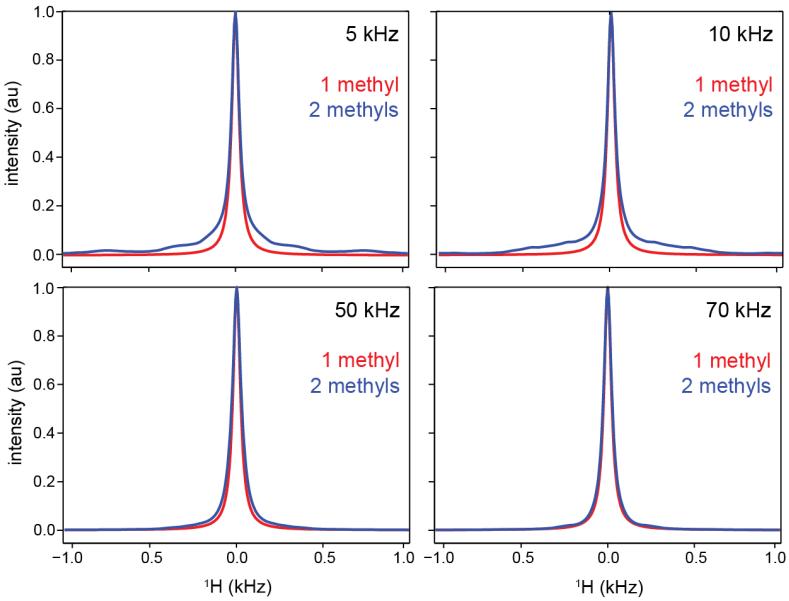

Figure 6. *MAS frequency dependence of the ^{1}H lineshape for an isolated single methyl (red) and one of two interacting methyl groups (blue). In the simulation, a chemical shift difference*

of 200 Hz, an inter-methyl proton-proton dipolar coupling of 2 kHz and the relative methyl-methyl orientations of Figure 5C are assumed. Figure adapted with permission from ref 81, ACS.

Next, we wanted to compare these simulations with experimental data. An α-spectrin SH3 sample was prepared using racemically labelled α–ketoisovalerate in the bacterial growth medium, implying a 50 % probability of incorporating $^{13}CH_3$ either into the pro-R or pro-S position for valine and leucine. The fact that the protonated methyl group is racemically incorporated into the side chain complicates the analysis. In the calculation, we have considered the two closest valine/leucine methyl groups in any given valine/leucine side chain pair, and have disregarded other configurations. This approach thus potentially overestimates dipolar interactions. Using the PDB structure (PDB ID: 2NUZ), all possible valine/leucine pair combinations found in the structure were analyzed. The simulated spectra obtained were subsequently averaged to yield the final proton spectrum for a given methyl group. Depending on the density of the dipolar coupling network, the search led to 4-17 variants per residue (for example, V44 Hγ1 yields 17 variants whereas L8 Hδ1 yields only 4 variants in the search for nearest neighbours to yield a 9- spin system) in the SH3 domain.

Figure 7A-E compares the simulations and experimental cross peak intensities for MAS frequencies of 70, 90 and 111 kHz. The $^{1}H,^{13}C$ correlation experiments were recorded employing INEPT-based polarization transfers[80, 81]. The T_2' signal decay times in the INEPT based experiments were measured independently. Simulated and experimental intensities are related by the following formula

$$\mathrm{INT}_j^{\exp}(i) = \kappa_j \mathrm{INT}_j^{sim}(i)\ \mathrm{e}^{-\Delta/T_2'} \qquad \text{Eq. [5]}$$

where κ_j represents a global scaling factor that is the same for all cross peaks in a particular spectrum *j* recorded at a particular MAS rotation frequency. κ_j can be found from the correlation plot shown in Figure 7A-C. Δ refers to the total INEPT magnetization transfer delay, which was set to 7.9 ms in all experiments.

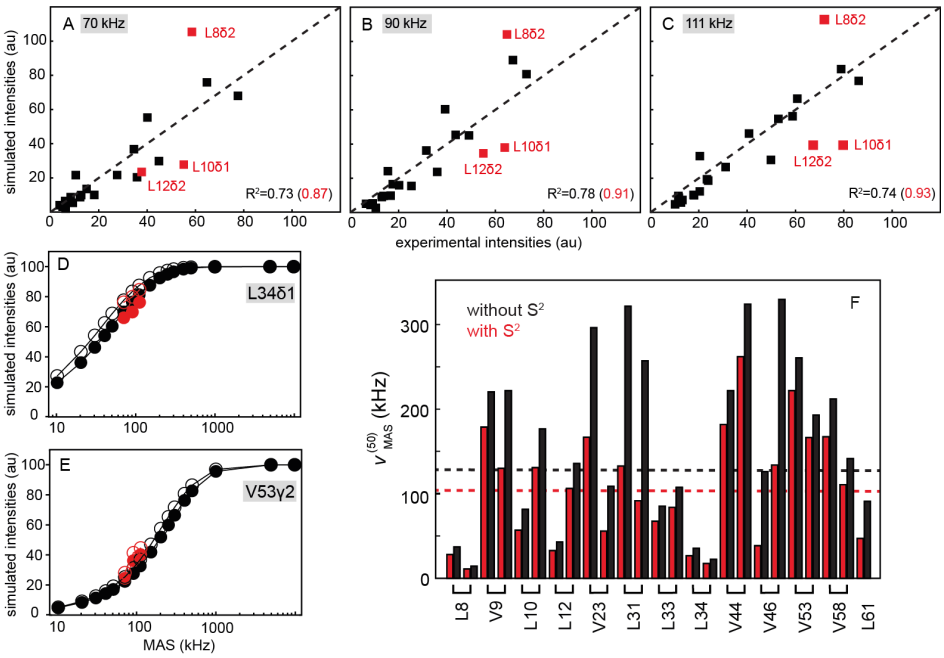

Figure 7. *Cross peak intensities in arbitrary units (au) are compared between simulation and experiments at MAS frequencies of 70 kHz(A), 90 kHz(B) and 111 kHz(C). Simulations were performed assuming an external magnetic field of 500 MHz. (D)-(E) L34δ1 and V53γ2 were chosen to show the agreement between experimental (red) and simulation (black) results. Closed and open symbols refer to simulations that were carried out assuming rigid side chains or accounting for dynamics, respectively. Order parameters for methyl dynamics were obtained from Asami et al [82]. (F) Characteristic MAS frequency $\nu_{MAS}^{(50)}$ as a function of residue. $\nu_{MAS}^{(50)}$ refers to the MAS rotation frequency that is needed to achieve 50% of the maximum intensity for a particular methyl group in the microcrystalline SH3 sample. The average characteristic MAS frequencies in the absence (black) and in the presence of dynamics (red) were (135.0 ± 88.0) kHz and (104.0 ± 68) kHz, respectively, where uncertainties quoted are 2σ, and are indicated with a dashed line. Figure adapted with permission from ref 81, ACS.*

Residues such as L34δ1 that experience weak local proton dipolar fields reach the maximum possible intensity at a lower MAS frequency (Figure 7D). On the other hand, residues that are buried inside the core of the protein and that experience strong proton dipolar interactions such as V53γ2 require much higher MAS frequencies to yield the maximum intensity (Figure 7E). Of note, at a MAS frequency of 110 kHz V53γ2 yields only ~40 % of the maximum possible intensity, whereas L34δ1 yields ~80%, which also explains the large variation in cross peak intensities visible in the ^{1}H, ^{13}C spectra shown in Figure 2.

To define the MAS frequency that is needed to reach 50 % of the maximum intensity, we introduce the empirical parameter $\nu_{MAS}^{(50)}$. $\nu_{MAS}^{(50)}$ ranges from as low as 20 kHz (L34δ2) up to 324 kHz (V53γ1), with an average value of 135.0 ± 88.0 kHz at an external magnetic field strength of 11.7 T (500 MHz) (Figure 7F). In the presence of side chain dynamics, ^{1}H-^{1}H dipolar couplings in the methyl groups are scaled. This results in an effectively reduced $\nu_{MAS}^{(50)}$ value of (104.0 ± 68) kHz. ^{1}H,^{13}C order parameters were measured for methyl groups using a REDOR-based experiment [83].

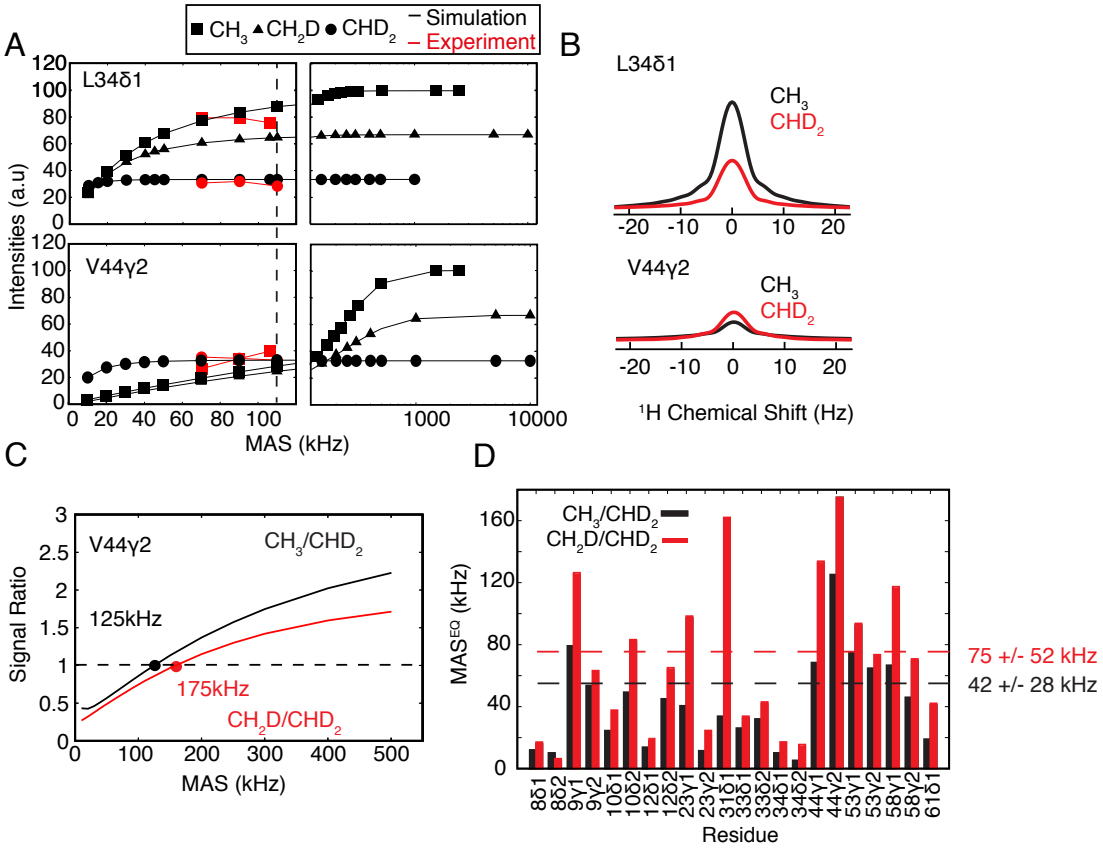

Figure 8. *A) Simulated (black) and experimental (red) proton peak intensities for L34δ1 and V44γ2 in α-spectrin SH3 as a function of MAS frequency for CHD_2, CH_2D and CH_3 labelled samples. Experimental intensities were corrected for the amounts of sample in the different rotors, employing a direct excitation 1D-^{13}C experiment for quantification. Experimental intensities were scaled by the appropriate κ_j [81]. B) Simulated proton lineshapes for the methyl groups L34δ1 and V44γ2. All simulations were carried out assuming a MAS frequency of 110 kHz and an external magnetic field of 1 GHz. Intensities are normalized according to the numbers of protons. C) Simulated intensity ratios for CH_3 vs. CHD_2 labelled samples (black) and for CH_2D vs. CHD_2 labelled samples (red) calculated as a function of MAS frequency for the V44γ2 methyl group. V44γ2 is located in the core of the protein and experiences the highest local proton density. D) MAS^{EQ} as a function of residue. MAS^{EQ} represents the MAS frequency*

that is necessary to achieve equal intensity in a CH_3 labelled sample versus a CHD_2 labelled sample (black), and CH_2D labelled sample versus a CHD_2 labelled sample (red). In all simulations, a B_0 field of 1 GHz is assumed. Figure adapted with permission from ref 84, Springer.

So far, we considered selectively methyl protonated samples. Given the fact that MAS frequencies on the order of 300 kHz are necessary to achieve 80 % of the maximum possible signal intensity on average, we also investigated how CHD_2 (and CH_2D) isotopomers compete with CH_3 in terms of sensitivity. Despite the fact that there are 3 protons in CH_3, the corresponding signal can be broad and thus yield low SNR.

$^{13}CH_3$ selective labeling is superior in terms of SNR when MAS frequencies over 100 kHz are available. However, the situation changes for lower MAS frequencies. For example, methyl CH_3 labeling yields 3-fold higher SNR for L34δ1 (Figure 8A and 8B) in SH3 for all MAS frequencies above 70 kHz, whereas CH_3 and CHD_2 isotopomers for V44γ2 yield equal intensity only if an MAS frequency of 125 kHz is employed [84]. By contrast, CH_2D isotopomers benefit in terms of SNR above a MAS frequency of 175 kHz (Figure 8C). Using numerical simulations, we calculate the minimum MAS frequency where CH_3/CHD_2 or CH_2D/CHD_2 isotopomers yield equal intensity (Figure 8D). On average, more than ~ 75 kHz MAS is necessary to yield higher SNR in SH3 employing CH_3 labelling, whereas MAS ~ 42 kHz is sufficient to yield equal intensity between CH_2D and CHD_2 isotopomers.
This information is potentially of interest for the design of experiments involving very large protein complexes for which sensitivity is limiting, and for which an additional gain in sensitivity would be desirable [30, 85-87].

Next, we address the effect of the external B_0 field on the SNR for ^1H, ^{13}C correlation experiments [88]. For the experiments, we employed a microcrystalline α-spectrin SH3 sample that again was produced using racemically labelled α-ketoisovalerate to yield 50% labelling each of the valine/leucine pro-R and pro-S methyl positions. The B_0 dependence is more complex than that predicted from Eq. [4], which simply represents the canonical $B_0^{3/2}$ behavior.

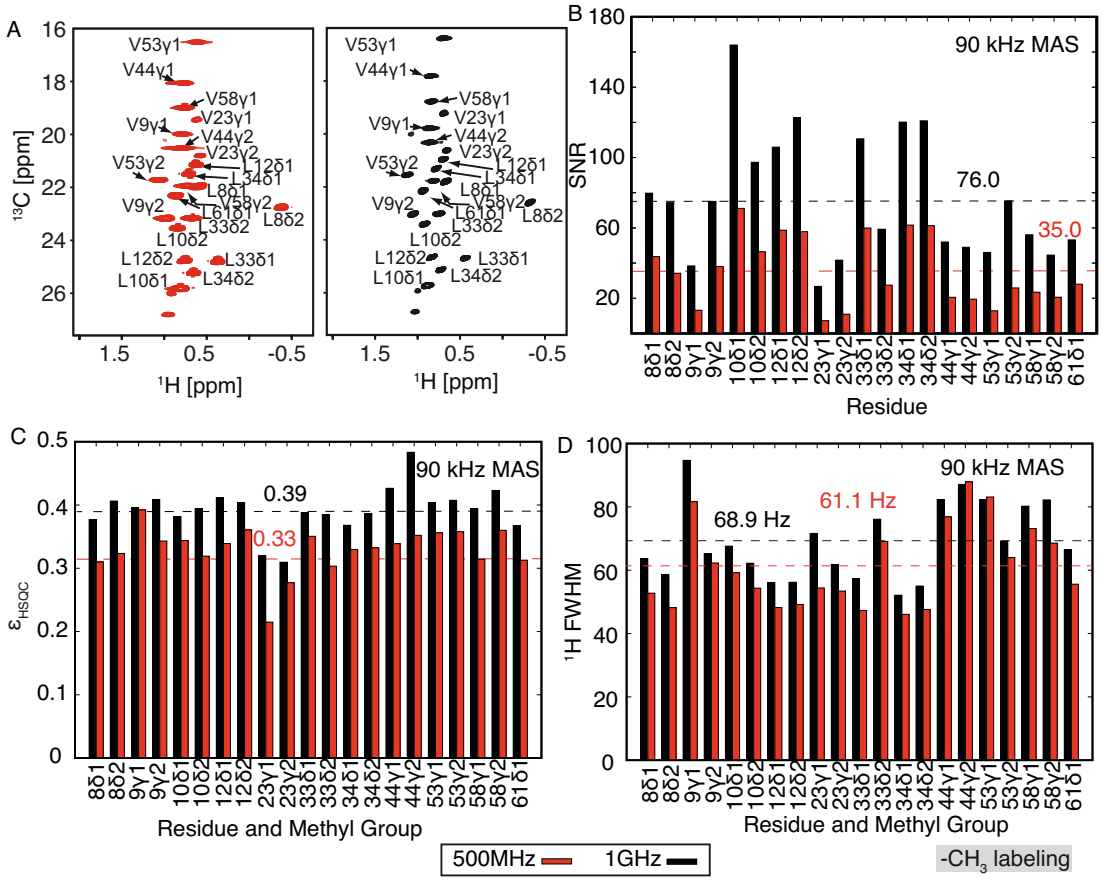

Figure 9. *(A) $^{1}H,^{13}C$ correlation spectra recorded at an MAS frequency of 90 kHz for a selectively valine and leucine methyl-protonated αSH3 domain sample, which is in either the pro-R and pro-S site. Measurements were performed at B_0 fields of 500 MHz (red) and 1 GHz (black). (B) The SNR of the cross peaks increases from a mean of 35:1 to 76:1 when the field is increased from 500 MHz to 1 GHz. (C) Site-specific polarization transfer efficiencies ε_{HCH} = $\varepsilon(H \rightarrow C) \times \varepsilon(C \rightarrow H)$ for Hartmann–Hahn-based cross polarization transfers at 500 MHz and 1 GHz. The transfer efficiencies are slightly higher at 1 GHz than at 500 MHz. (D) Proton linewidth as a function of residue. The mean linewidth (FWHM) at 1 GHz is slightly larger compared to the linewidth obtained from spectra recorded at 500 MHz. Figure adapted with permission from ref 88, ACS.*

$^{1}H,^{13}C$ Correlation spectra for a CH_3 labelled SH3 sample were recorded for B_0 fields of 500 MHz and 1 GHz (Figure 9A). After measuring the peak heights, the SNR is compared (Figure 9B). On average, the SNR increases from 35 to 76, *i.e.*, is ~2.2 times higher when experiments are carried out at 1 GHz compared to 500 MHz [88]. In addition to $B_0^{3/2}$ (~ 2.8 times in this case), other factors that contribute to the SNR are the coherence transfer efficiency ε_{HCH}, the linewidths in the ^{1}H and ^{13}C dimensions and general contributions from hardware (Figure 9D). We find that ε_{HCH} and the ^{1}H and ^{13}C

linewidths are larger at 1 GHz than at 500 MHz (1 GHz: ε_{HCH} ~0.39, mean ^{1}H FWHM ~68.9 Hz, mean ^{13}C FWHM ~21.4 Hz; 500 MHz: ε_{HCH} ~0.33, mean ^{1}H FWHM ~61.1 Hz, mean ^{13}C FWHM ~14.8 Hz). For residues that are deeply buried inside the core of the protein (such as V9, V23 and V53) and that have in general a very low absolute sensitivity, the gain in SNR can exceed the prediction from Eq. [4] by ~2x at high B_0 fields (Figure 10). For other residues such as L10, L33 and L34, the agreement with Eq. [4] is excellent.

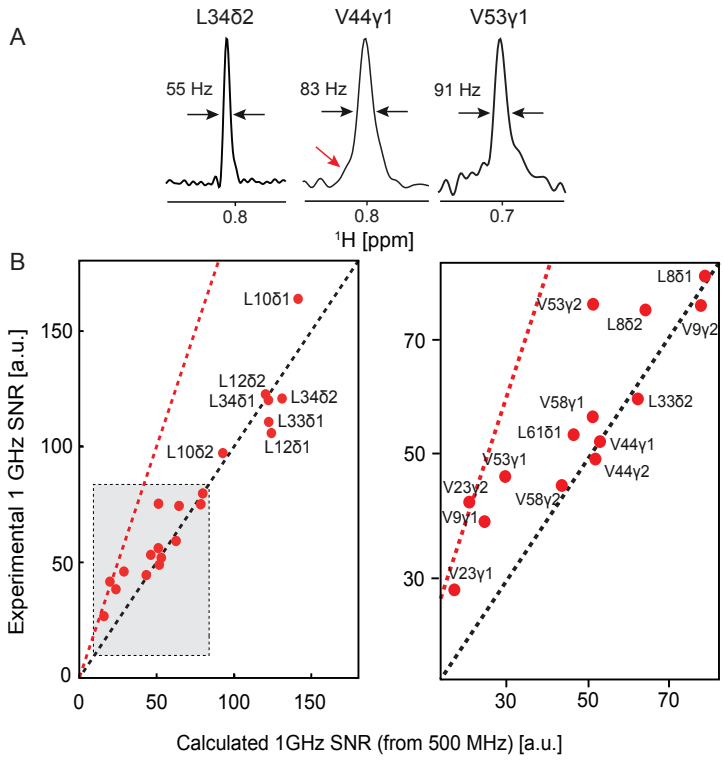

Figure 10. *1D traces from ^{1}H,^{13}C correlation spectra along the proton dimension for the methyl cross-peaks L34δ2, V44γ1 and V53γ1. Spectra were recorded at 1 GHz using a selectively valine and leucine methyl protonated αSH3 domain sample. The red arrow for V44γ1 highlights a broad component in the base of the peak. (B) Correlation of the experimental intensity at 1 GHz (vertical axis) and the predicted intensity (horizontal axis) using intensity values obtained at 500 MHz and by using the relation* $SNR_{1GHz} = SNR_{500MHz} * (\frac{LW(C)_{500MHz} * LW(H)_{500MHz}}{LW(C)_{1GHz} * LW(H)_{1GHz}}) * (\frac{\epsilon_{1GHz}}{\epsilon_{500MHz}}) * \left(\frac{1000}{500}\right)^{3/2}$. *For peaks with relatively high intensity, a good correlation is observed (the black dashed line plots y = x). For peaks with relatively low intensity, however, the experimental intensities at 1 GHz are significantly higher than expected from the 500 MHz data (shaded region; magnified in the right-hand side panel, red, dashed line at y=2*x). Figure adapted with permission from ref 88, ACS.*

In order to understand the origin of the gain in SNR at high B_0 fields, we investigated the shape of the proton resonances in more detail. In simulations, we find that the proton resonances feature a narrow component, and a broad component at the base of the peak (Figures 5, 6). Due to the limitations in sensitivity, it is difficult to observe the broad features of the resonance experimentally. Phenomenologically, the decay of the resonance under the influence of the coherent part of the Hamiltonian is determined by a slow ($T_2^{coh,slow}$) and a fast ($T_2^{coh,fast}$) component which are weighted by p_1 and p_2, respectively.

$$S(t) = \left\{ p_1 \times exp\left(-\frac{t}{T_2^{coh,fast}}\right) + p_2 \times exp\left(-\frac{t}{T_2^{coh,slow}}\right)\right\} \qquad \text{Eq. [6]}$$

with $p_1 + p_2 = 1$

The coherent processes are functions of MAS frequency, chemical shifts of protons, and the dipolar interaction between the nearest pair of protons, and give rise to a slow ($T_2^{coh,slow}$) and a fast decay ($T_2^{coh,fast}$) of the proton signal. Chávez et al. [89] have employed single mode Floquet theory to analyse the coherent linewidths of proton resonances for spinning solids that also show a complex dependence on molecular parameters.

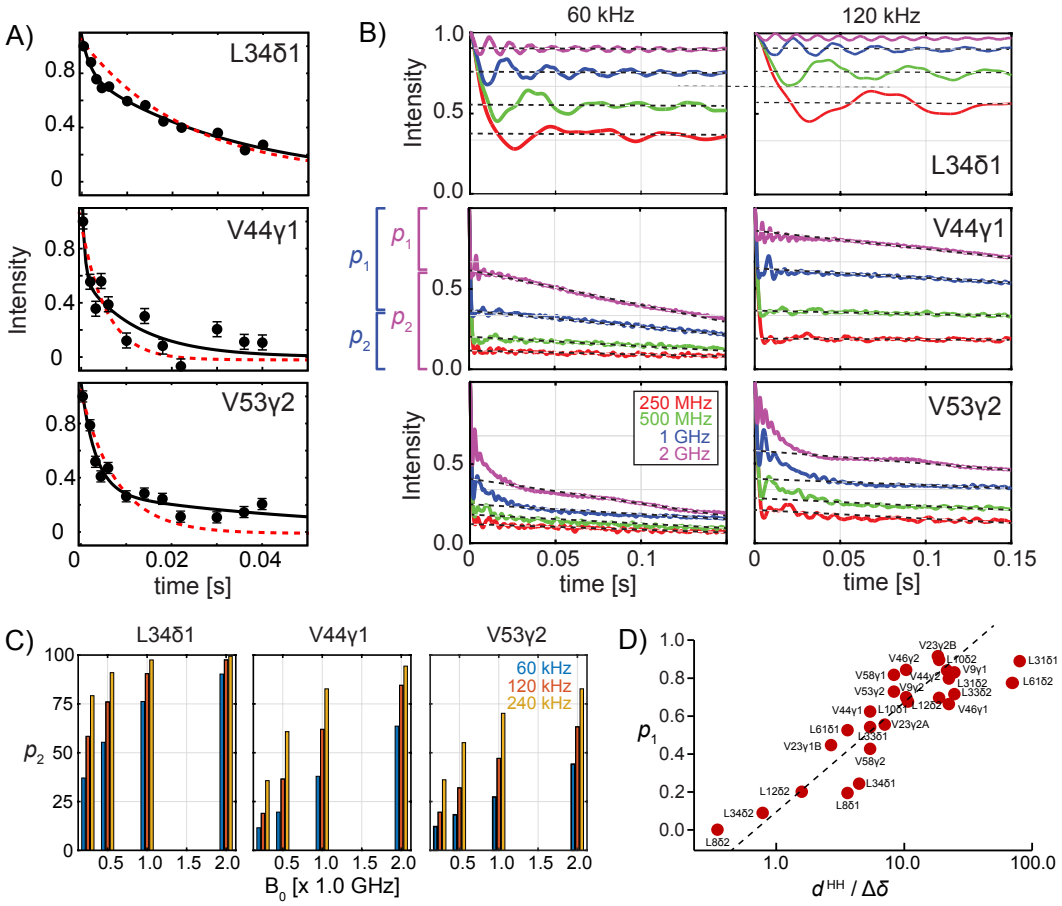

***Figure 11**. A) Experimental ¹H-T_2' decay curves for a few representative residues in the microcrystalline selectively CH_3 protonated αSH3 sample Multi-exponential fits (monoexponential, solid black lines; biexponential, dotted red lines) are required to adequately describe the experimental data. B) SIMPSON simulations of ¹H Hahn echo experiments for L34 δ1, V44γ1, V53γ2 assuming the exact geometry of the αSH3 domain (PDB ID: 2NUZ). For the simulations, 9 proton spins have been taken into account. The parameters p1 and p2 are employed to describe the simulations empirically. C) The slowly decaying component p2 is shown as a function of B_0 and MAS frequency. D) Correlation of p1 and $d^{HH}/\Delta\delta$ assuming a magnetic field strength of 1 GHz. Figure adapted with permission from ref 88, ACS.*

It is difficult to distinguish experimentally between the different coherent decay processes. However, SIMPSON simulations were again carried out assuming that a particular methyl group interacts with two neighbouring methyl groups. However, the SIMPSON simulations were again carried out assuming that a particular methyl group interacts with two neighbouring methyl groups. Simulations were performed as a function of the B_0 field and the MAS frequency. Figure 11B shows the simulated ¹H-T_2' decay curves for L34δ1, V44γ1 and V53γ2 at a MAS rotation frequency of 60 and 120 kHz and for the static magnetic fields of 250 MHz, 500 MHz, 1 GHz and 2 GHz. As in

the experiment, the simulations show that magnetization decays bi-exponentially. Next, the simulations were fitted employing Eq. [6], but omitting the incoherent contribution that is proportional to p_0.

The B_0 dependence of the slowly decaying component p_2 in the simulated data of Fig. 11B is shown in Figure 11C. At higher magnetic fields, chemical shifts are separated by greater frequency differences. The contribution of the slowly decaying component to the spin echo signal increases under these conditions. In particular, p_2 increases from 0.19 to 0.64 for V53γ2 when the magnetic field increases from 250 MHz to 2 GHz at a fixed MAS frequency of 120 kHz. Faster MAS facilitates averaging of proton-proton dipolar interactions. For V53γ2, p_2 has a value of 0.55 at a MAS frequency of 240 kHz and a static field of 500 MHz, while p_2 is as low as 0.27 at a MAS frequency of 60 kHz at a static B_0 field of 1 GHz. L34δ2 is a methyl group that is only weakly coupled with other protons. As a consequence, p_2 already reaches a value of 0.9 at a MAS frequency and B_0 field of 120 kHz and 1 GHz, respectively.

We assume that the rapidly-decaying component depends on the proton-proton dipolar coupling d^{HH} and the chemical shift difference to the strongest coupling partner Δδ. Of note, d^{HH} is different from d^{RSS}, as the latter denotes the root mean squared sum of all dipolar couplings. We have therefore represented p_1 as a function of $d^{HH}/\Delta\delta$ (Figure 11D). In the simulation, a static magnetic field B_0 of 1 GHz is assumed. We find that p_1 correlates well with $d^{HH}/\Delta\delta$. For $d^{HH}/\Delta\delta < 1$, the rapidly-decaying component in fact vanishes. V53γ2 is densely packed in the core of the α-SH3 domain. The closest methyl is V58γ1. The two methyl groups exhibit a mutual dipolar coupling of $d^{HH}/2\pi$ ~ 2392 Hz, and a chemical shift difference of $\Delta\delta$ ~ 288 Hz at 1 GHz, yielding $d^{HH}/\Delta\delta$ ~ 9. The spin echo decay for V53γ2 yields a significantly higher p_1 ~ 0.7 compared to L34δ2, for which $d^{HH}/\Delta\delta$ is on the order of ~ 0.9 (p_1 ~ 0.08; $d^{HH}/2\pi$ ~237 Hz, while $\Delta\delta$ ~303 Hz at 1 GHz).

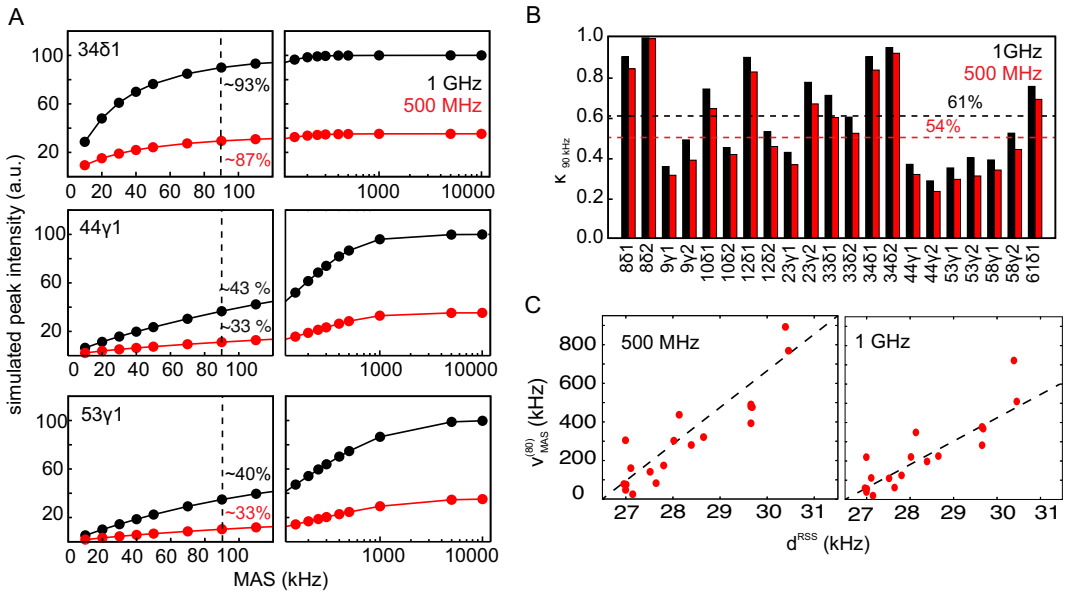

Figure 12. *(A) Simulated MAS frequency dependence of methyl proton intensities for L34δ2, V44γ1 and V53γ1, assuming B_0 fields of 500 MHz and 1 GHz, respectively. In the calculation, it is assumed that only valine and leucine methyl groups of αSH3 are labelled as $^{13}CH_3$, while the rest of the protein is deuterated. As expected, a systematically higher signal to noise ratio is obtained for 1 GHz compared to 500 MHz due to the effect of static magnetic field. The percentages in figure B (κ_{90kHz}) indicate the fraction of the maximum achievable sensitivity obtained at a MAS frequency of 90 kHz (dashed lines). (B) κ_{90kHz} for each methyl group in α-SH3 calculated for magnetic field strengths of 500 MHz (red) and 1 GHz (black). (C) Correlation of the characteristic MAS frequency necessary to obtain 80 % of the maximum achievable intensity $\nu_{MAS}^{(80)}$ versus the effective dipolar coupling d^{RSS} at 500 MHz (left) and 1 GHz (right). The slope of the correlation plot decreases for higher fields, suggesting that high fields facilitate line narrowing by magic angle spinning. Figure adapted with permission from ref 88, ACS.*

Figure 12A shows the simulated signal intensities as a function of B_0 and MAS frequency for a few representative residues. Obviously, higher intensities are obtained at higher magnetic field strengths. In order to appreciate how the intensity of a particular methyl group relates to the maximum possible sensitivity, we introduce the parameter κ_{90kHz}. κ_{90kHz} refers to the fraction of the maximum achievable sensitivity obtained at a MAS frequency of 90 kHz. Maximum achievable intensity is defined by the intensity at a given B_0 field where all anisotropic interactions are completely averaged out by sufficiently fast MAS. For V53γ1, κ_{90kHz} amounts to ~ 33% at 500 MHz, while this value increases to κ_{90kHz} ~ 40% at a field of 1 GHz. Similarly, κ_{90kHz} is equal

to 87% and 93% for L34δ2 at B_0 fields of 500 MHz and 1 GHz, respectively. On average, κ_{90kHz} is on the order of ~ 54% at a B_0 of 500 MHz, while increasing to ~ 61% at a B_0 field of 1 GHz (Figure 12B). This indicates that high magnetic fields imply gains in sensitivity that are beyond the canonical $B_0^{3/2}$ dependence. Figure 12C shows a correlation between the characteristic MAS frequency $\nu^{(80)}_{MAS}$ and the effective dipolar coupling d^{RSS} for α-SH3. The characteristic MAS frequency is defined as the frequency which is required to obtain 80 % of the maximum intensity for a given methyl group. Again, higher magnetic fields facilitate MAS induced averaging of proton dipolar couplings.

Conclusion

The signal to noise ratio (SNR) is one of the principal factors determining the quality of NMR spectra. Sensitivity is a function of several important parameters, including the external magnetic field strength, the gyromagnetic ratio of the detected nucleus, and the linewidth, omitting for the moment the contributions from hardware components. Linewidths of resonances originate from homogeneous and inhomogeneous interactions, and change as a function of the MAS frequency, the homogeneity of the sample, and the strength of the dipolar coupling network among the protons. Using experiments employing different levels of deuteration and numerical simulations, we have shown that for a CH_3 selectively protonated SH3 sample, MAS frequencies on the order of (135.0 ± 88.0) kHz at an external magnetic field strength of 11.7 T (500 MHz) are necessary to yield at least 50 % of the maximum possible intensity in $^{1}H,^{13}C$ correlation experiments. Spectra obtained at higher B_0 fields improve SNR by decreasing the ratio of the dipolar coupling to the chemical shift difference ($d^{HH}/\Delta\delta$), inducing a transition from a strong into a weak coupling limit. A quantitative description of the proton network around a given nucleus is difficult. d^{RSS} contains information only on the magnitude of the dipolar coupling among all coupling partners. Numerical simulations have shown, however, that the proton lineshape depends heavily on the relative orientation of the dipolar coupling tensors.

SNR can also benefit from cryogenically cooled solid state NMR probes[90], novel designs of MAS rotors[91] or RF coils[92] with enhanced quality factors producing homogeneous RF fields over sample volume, and faster MAS and higher B_0 fields. The maximum MAS frequency is determined by the speed of sound on the surface of the

rotor in a particular medium. Helium-driven MAS rotors [93] are one possible way to achieve the same MAS frequency with larger volume rotors. This allows the possibility to employ more material for the NMR experiment at a given MAS frequency and thus increase sensitivity, in comparison to a setup in which nitrogen gas is used for sample rotation. With the recent installation of 28.2 T magnets (^{1}H Larmor frequency of 1.2 GHz), high B_0 fields are becoming available for proton detected biological solid-state NMR experiments [94] [95]. It has been shown that the linewidths of amide and Hα protons in ppm decrease linearly with the field, reducing chemical shift overlap and facilitating resonance assignment. Due to the reduced values for $d^{HH}/\Delta\delta$ at high fields, lines as narrow as a few Hertz are observed. It remains to be seen to which limits MAS rotation frequencies can be further increased. Certainly, biological solid-state NMR will benefit both from increases in external B_0 field and improvements in magic angle spinning.

Acknowledgement

We thank Venita Decker and Sebastian Wegner from Bruker Biospin, Karlsruhe and Daniela Lalli, Guido Pintacuda in ENS Lyon for providing access to spectrometers and 0.7mm MAS probes. This work was performed in the framework of the SFB-1035 (Project B07; German Research Foundation, DFG). We acknowledge support from the Helmholtz-Gemeinschaft, the Deutsche Forschungsgemeinschaft (DFG, Grant Re1435), the Center for Integrated Protein Science Munich (CIPS-M), the Czech Science Foundation (grant no. 20-00166J (ZT)). Computational resources were supplied by the project "e-Infrastruktura CZ" (e-INFRA CZ ID:90140) supported by the Ministry of Education, Youth and Sports of the Czech Republic.

Reference

[1] Andrew ER, Bradbury A, Eades RG. Nuclear Magnetic Resonance Spectra from a Crystal rotated at High Speed. Nature. 1958;182:1659-.
[2] Lowe IJ. Free Induction Decays of Rotating Solids. Physical Review Letters. 1959;2:285-7.
[3] McDermott AE, Creuzet FJ, Kolbert AC, Griffin RG. High-resolution magic-angle-spinning NMR spectra of protons in deuterated solids. Journal of Magnetic Resonance (1969). 1992;98:408-13.

[4] Zheng L, Fishbein KW, Griffin RG, Herzfeld J. Two-dimensional solid-state proton NMR and proton exchange. Journal of the American Chemical Society. 1993;115:6254-61.
[5] Chevelkov V, van Rossum BJ, Castellani F, Rehbein K, Diehl A, Hohwy M, et al. 1H Detection in MAS Solid-State NMR Spectroscopy of Biomacromolecules Employing Pulsed Field Gradients for Residual Solvent Suppression⊥. Journal of the American Chemical Society. 2003;125:7788-9.
[6] Paulson EK, Morcombe CR, Gaponenko V, Dancheck B, Byrd RA, Zilm KW. Sensitive high resolution inverse detection NMR spectroscopy of proteins in the solid state. J Am Chem Soc. 2003;125:15831-6.
[7] Reif B, Griffin RG. 1H detected 1H,15N correlation spectroscopy in rotating solids. Journal of Magnetic Resonance. 2003;160:78-83.
[8] Reif B, Jaroniec CP, Rienstra CM, Hohwy M, Griffin RG. 1H–1H MAS Correlation Spectroscopy and Distance Measurements in a Deuterated Peptide. Journal of Magnetic Resonance. 2001;151:320-7.
[9] Schubeis T, Le Marchand T, Andreas LB, Pintacuda G. 1H magic-angle spinning NMR evolves as a powerful new tool for membrane proteins. Journal of Magnetic Resonance. 2018;287:140-52.
[10] Chevelkov V, Rehbein K, Diehl A, Reif B. Ultrahigh Resolution in Proton Solid-State NMR Spectroscopy at High Levels of Deuteration. Angewandte Chemie International Edition. 2006;45:3878-81.
[11] Agarwal V, Diehl A, Skrynnikov N, Reif B. High Resolution1H Detected1H,13C Correlation Spectra in MAS Solid-State NMR using Deuterated Proteins with Selective1H,2H Isotopic Labeling of Methyl Groups. Journal of the American Chemical Society. 2006;128:12620-1.
[12] Agarwal V, Xue Y, Reif B, Skrynnikov NR. Protein Side-Chain Dynamics As Observed by Solution- and Solid-State NMR Spectroscopy: A Similarity Revealed. Journal of the American Chemical Society. 2008;130:16611-21.
[13] Asami S, Schmieder P, Reif B. High Resolution 1H-Detected Solid-State NMR Spectroscopy of Protein Aliphatic Resonances: Access to Tertiary Structure Information. Journal of the American Chemical Society. 2010;132:15133-5.
[14] Knight MJ, Webber AL, Pell AJ, Guerry P, Barbet-Massin E, Bertini I, et al. Fast Resonance Assignment and Fold Determination of Human Superoxide Dismutase by High-Resolution Proton-Detected Solid-State MAS NMR Spectroscopy. Angewandte Chemie International Edition. 2011;50:11697-701.
[15] Lewandowski JR, Dumez J-N, Akbey Ü, Lange S, Emsley L, Oschkinat H. Enhanced Resolution and Coherence Lifetimes in the Solid-State NMR Spectroscopy of Perdeuterated Proteins under Ultrafast Magic-Angle Spinning. The Journal of Physical Chemistry Letters. 2011;2:2205-11.
[16] Akbey Ü, Lange S, Trent Franks W, Linser R, Rehbein K, Diehl A, et al. Optimum levels of exchangeable protons in perdeuterated proteins for proton detection in MAS solid-state NMR spectroscopy. Journal of Biomolecular NMR. 2009;46:67-73.
[17] Jekhmane S, Prachar M, Pugliese R, Fontana F, Medeiros-Silva J, Gelain F, et al. Design Parameters of Tissue-Engineering Scaffolds at the Atomic Scale. Angewandte Chemie. 2019;131:17099-107.
[18] Wiegand T, Schledorn M, Malär AA, Cadalbert R, Däpp A, Terradot L, et al. Nucleotide Binding Modes in a Motor Protein Revealed by 31P- and 1H-Detected MAS Solid-State NMR Spectroscopy. ChemBioChem. 2019;21:324-30.
[19] Zhang R, Hong Y-l, Ravula T, Nishiyama Y, Ramamoorthy A. High-resolution proton-detected MAS experiments on self-assembled diphenylalanine nanotubes

enabled by fast MAS and high magnetic field. Journal of Magnetic Resonance. 2020;313.
[20] Zhang R, Nishiyama Y, Ramamoorthy A. Exploiting heterogeneous time scale of dynamics to enhance 2D HETCOR solid-state NMR sensitivity. Journal of Magnetic Resonance. 2019;309.
[21] Vasa SK, Rovó P, Linser R. Protons as Versatile Reporters in Solid-State NMR Spectroscopy. Accounts of Chemical Research. 2018;51:1386-95.
[22] Vasa SK, Singh H, Grohe K, Linser R. Assessment of a Large Enzyme–Drug Complex by Proton-Detected Solid-State NMR Spectroscopy without Deuteration. Angewandte Chemie International Edition. 2019;58:5758-62.
[23] Linser R, Dasari M, Hiller M, Higman V, Fink U, Lopez del Amo J-M, et al. Proton-Detected Solid-State NMR Spectroscopy of Fibrillar and Membrane Proteins. Angewandte Chemie International Edition. 2011;50:4508-12.
[24] Lopez del Amo JM, Schmidt M, Fink U, Dasari M, Fändrich M, Reif B. An Asymmetric Dimer as the Basic Subunit in Alzheimer's Disease Amyloid β Fibrils. Angewandte Chemie International Edition. 2012;51:6136-9.
[25] Agarwal V, Linser R, Dasari M, Fink U, del Amo J-ML, Reif B. Hydrogen bonding involving side chain exchangeable groups stabilizes amyloid quarternary structure. Physical Chemistry Chemical Physics. 2013;15.
[26] Linser R, Sarkar R, Krushelnitzky A, Mainz A, Reif B. Dynamics in the solid-state: perspectives for the investigation of amyloid aggregates, membrane proteins and soluble protein complexes. Journal of Biomolecular NMR. 2014;59:1-14.
[27] Xiang S, Kulminskaya N, Habenstein B, Biernat J, Tepper K, Paulat M, et al. A Two-Component Adhesive: Tau Fibrils Arise from a Combination of a Well-Defined Motif and Conformationally Flexible Interactions. Journal of the American Chemical Society. 2017;139:2639-46.
[28] Smith AA, Ernst M, Riniker S, Meier BH. Localized and Collective Motions in HET-s(218-289) Fibrils from Combined NMR Relaxation and MD Simulation. Angewandte Chemie International Edition. 2019;58:9383-8.
[29] Niu Z, Prade E, Malideli E, Hille K, Jussupow A, Mideksa YG, et al. Structural Insight into IAPP-Derived Amyloid Inhibitors and Their Mechanism of Action. Angewandte Chemie International Edition. 2020;59:5771-81.
[30] Kurauskas V, Crublet E, Macek P, Kerfah R, Gauto DF, Boisbouvier J, et al. Sensitive proton-detected solid-state NMR spectroscopy of large proteins with selective CH3labelling: application to the 50S ribosome subunit. Chemical Communications. 2016;52:9558-61.
[31] Struppe J, Quinn CM, Lu M, Wang M, Hou G, Lu X, et al. Expanding the horizons for structural analysis of fully protonated protein assemblies by NMR spectroscopy at MAS frequencies above 100 kHz. Solid State Nuclear Magnetic Resonance. 2017;87:117-25.
[32] Lecoq L, Schledorn M, Wang S, Smith-Penzel S, Malär AA, Callon M, et al. 100 kHz MAS Proton-Detected NMR Spectroscopy of Hepatitis B Virus Capsids. Frontiers in Molecular Biosciences. 2019;6.
[33] Lu M, Wang M, Struppe J, Maas W, Gronenborn A, Polenova T. Towards Atomic-Resolution Structure Determination of HIV-1 Capsid Assemblies using Magic Angle Spinning NMR. Biophysical Journal. 2019;116.
[34] Böckmann A, Ernst M, Meier BH. Spinning proteins, the faster, the better? Journal of Magnetic Resonance. 2015;253:71-9.
[35] Callon M, Malär AA, Pfister S, Rímal V, Weber ME, Wiegand T, et al. 2021.

[36] Penzel S, Oss A, Org M-L, Samoson A, Böckmann A, Ernst M, et al. Spinning faster: protein NMR at MAS frequencies up to 126 kHz. Journal of Biomolecular NMR. 2019;73:19-29.
[37] Andreas LB, Jaudzems K, Stanek J, Lalli D, Bertarello A, Le Marchand T, et al. Structure of fully protonated proteins by proton-detected magic-angle spinning NMR. Proceedings of the National Academy of Sciences. 2016;113:9187-92.
[38] Xue K, Sarkar R, Motz C, Asami S, Camargo DCR, Decker V, et al. Limits of Resolution and Sensitivity of Proton Detected MAS Solid-State NMR Experiments at 111 kHz in Deuterated and Protonated Proteins. Scientific Reports. 2017;7.
[39] Ishii Y, Tycko R. Sensitivity Enhancement in Solid State 15N NMR by Indirect Detection with High-Speed Magic Angle Spinning. Journal of Magnetic Resonance. 2000;142:199-204.
[40] Abragam A. Principles of Nuclear Magnetism. New York: Oxford University Press; 1961.
[41] Ernst RR, Bodenhausen G, Wokaun A. Principles of Nuclear Magnetic Resonance in One and Two Dimensions. Oxford: Oxford University Press; 1987.
[42] Barbet-Massin E, Pell AJ, Retel JS, Andreas LB, Jaudzems K, Franks WT, et al. Rapid proton-detected NMR assignment for proteins with fast magic angle spinning. Journal of the American Chemical Society. 2014;136:12489-97.
[43] Hoult DI. The Principle of Reciprocity in Signal Strength Calculatios- A Mathematical Guide. Concepts in Magnetic Resonance. 2000;124.
[44] Kovacs H, Moskau D, Spraul M. Cryogenically cooled probes—a leap in NMR technology. Progress in Nuclear Magnetic Resonance Spectroscopy. 2005;46:131-55.
[45] Bryce DL, Bernard GM, Gee M, Lumsden MD, Eichele K, Wasylishen RE. Practical Aspects of Modern Routine Solid-State Multinuclear Magnetic Resonance Spectroscopy: One-Dimensional Experiments. ChemInform. 2010;33:46-82.
[46] Earl WL, Vanderhart DL. Measurement of 13C chemical shifts in solids. Journal of Magnetic Resonance (1969). 1982;48:35-54.
[47] Carravetta M, Danquigny A, Mamone S, Cuda F, Johannessen OG, Heinmaa I, et al. Solid-state NMR of endohedral hydrogen–fullerene complexes. Physical Chemistry Chemical Physics. 2007;9.
[48] Komatsu K. Encapsulation of Molecular Hydrogen in Fullerene C60 by Organic Synthesis. Science. 2005;307:238-40.
[49] Matsuo Y, Isobe H, Tanaka T, Murata Y, Murata M, Komatsu K, et al. Organic and Organometallic Derivatives of Dihydrogen-Encapsulated [60]Fullerene. Journal of the American Chemical Society. 2005;127:17148-9.
[50] Bertini I, Luchinat C, Parigi G, Ravera E, Reif B, Turano P. Solid-state NMR of proteins sedimented by ultracentrifugation. Proceedings of the National Academy of Sciences. 2011;108:10396-9.
[51] Mainz A, Jehle S, van Rossum BJ, Oschkinat H, Reif B. Large Protein Complexes with Extreme Rotational Correlation Times Investigated in Solution by Magic-Angle-Spinning NMR Spectroscopy. Journal of the American Chemical Society. 2009;131:15968-9.
[52] Bertini I, Engelke F, Gonnelli L, Knott B, Luchinat C, Osen D, et al. On the use of ultracentrifugal devices for sedimented solute NMR. Journal of Biomolecular NMR. 2012;54:123-7.
[53] Bertini I, Luchinat C, Parigi G, Ravera E. SedNMR: On the Edge between Solution and Solid-State NMR. Accounts of Chemical Research. 2013;46:2059-69.

[54] Böckmann A, Gardiennet C, Verel R, Hunkeler A, Loquet A, Pintacuda G, et al. Characterization of different water pools in solid-state NMR protein samples. Journal of Biomolecular NMR. 2009;45:319-27.
[55] Gardiennet C, Schütz AK, Hunkeler A, Kunert B, Terradot L, Böckmann A, et al. A Sedimented Sample of a 59 kDa Dodecameric Helicase Yields High-Resolution Solid-State NMR Spectra. Angewandte Chemie International Edition. 2012;51:7855-8.
[56] Hisao GS, Harland MA, Brown RA, Berthold DA, Wilson TE, Rienstra CM. An efficient method and device for transfer of semisolid materials into solid-state NMR spectroscopy rotors. Journal of Magnetic Resonance. 2016;265:172-6.
[57] Mandal A, Boatz JC, Wheeler TB, van der Wel PCA. On the use of ultracentrifugal devices for routine sample preparation in biomolecular magic-angle-spinning NMR. Journal of Biomolecular NMR. 2017;67:165-78.
[58] Stevens RA. The development of solid-state NMR methodology to study the dynamics of proteins and ice [PhD Thesis]: University of Warwick; 2018.
[59] Maricq MM, Waugh JS. NMR in rotating solids. The Journal of Chemical Physics. 1979;70:3300-16.
[60] Garroway AN, Vanderhart DL, Earl WL. 13C NMR in organic solids: limits to spectral resolution and to determination of molecular motion. Philosophical Transactions of the Royal Society of London Series A, Mathematical and Physical Sciences. 1981;299:609-28.
[61] Vanderhart DL, Earl WL, Garroway AN. Resolution in 13C NMR of organic solids using high-power proton decoupling and magic-angle sample spinning. Journal of Magnetic Resonance (1969). 1981;44:361-401.
[62] Hodgkinson P. High-Resolution 1H NMR Spectroscopy of Solids. Annual Reports on NMR Spectroscopy2011. p. 185-223.
[63] Zhou DH, Graesser DT, Franks WT, Rienstra CM. Sensitivity and resolution in proton solid-state NMR at intermediate deuteration levels: Quantitative linewidth characterization and applications to correlation spectroscopy. Journal of Magnetic Resonance. 2006;178:297-307.
[64] Zorin VE, Brown SP, Hodgkinson P. Origins of linewidth in 1H magic-angle spinning NMR. J Chem Phys. 2006;125:144508.
[65] Samoson A, Tuherm T, Gan Z. High-Field High-Speed MAS Resolution Enhancement in 1H NMR Spectroscopy of Solids. Solid State Nuclear Magnetic Resonance. 2001;20:130-6.
[66] Zorin VE, Brown SP, Hodgkinson P. Quantification of homonuclear dipolar coupling networks from magic-angle spinning1H NMR. Molecular Physics. 2006;104:293-304.
[67] Kuprov I. Fokker-Planck formalism in magnetic resonance simulations. Journal of Magnetic Resonance. 2016;270:124-35.
[68] Sternberg U, Witter R, Kuprov I, Lamley JM, Oss A, Lewandowski JR, et al. 1 H line width dependence on MAS speed in solid state NMR – Comparison of experiment and simulation. Journal of Magnetic Resonance. 2018;291:32-9.
[69] Malär AA, Smith-Penzel S, Camenisch G-M, Wiegand T, Samoson A, Böckmann A, et al. Quantifying proton NMR coherent linewidth in proteins under fast MAS conditions: a second moment approach. Physical Chemistry Chemical Physics. 2019;21:18850-65.
[70] Van Vleck JH. The Dipolar Broadening of Magnetic Resonance Lines in Crystals. Physical Review. 1948;74:1168-83.
[71] Ollerenshaw JE, Tugarinov V, Kay LE. Methyl TROSY: explanation and experimental verification. Magnetic Resonance in Chemistry. 2003;41:843-52.

[72] Sprangers R, Kay LE. Quantitative dynamics and binding studies of the 20S proteasome by NMR. Nature. 2007;445:618-22.
[73] Sprangers R, Velyvis A, Kay LE. Solution NMR of supramolecular complexes: providing new insights into function. Nature Methods. 2007;4:697-703.
[74] Andreas LB, Jaudzems K, Stanek J, Lalli D, Bertarello A, Le Marchand T, et al. Structure of fully protonated proteins by proton-detected magic-angle spinning NMR. Proc Natl Acad Sci U S A. 2016;113:9187-92.
[75] Agarwal V, Penzel S, Szekely K, Cadalbert R, Testori E, Oss A, et al. De novo 3D structure determination from sub-milligram protein samples by solid-state 100 kHz MAS NMR spectroscopy. Angew Chem Int Ed Engl. 2014;53:12253-6.
[76] Tugarinov V, Kay LE. Ile, Leu, and Val Methyl Assignments of the 723-Residue Malate Synthase G Using a New Labeling Strategy and Novel NMR Methods. Journal of the American Chemical Society. 2003;125:13868-78.
[77] Bak M, Rasmussen JT, Nielsen NC. SIMPSON: A General Simulation Program for Solid-State NMR Spectroscopy. Journal of Magnetic Resonance. 2000;147:296-330.
[78] Tošner Z, Andersen R, Stevensson B, Edén M, Nielsen NC, Vosegaard T. Computer-intensive simulation of solid-state NMR experiments using SIMPSON. Journal of Magnetic Resonance. 2014;246:79-93.
[79] Maricq MM, Waugh JS. NMR in rotating solids. J Chem Phys. 1979;70:3300-16.
[80] Morris GA, Freeman R. Enhancement of nuclear magnetic resonance signals by polarization transfer. Journal of the American Chemical Society. 1979;101:760-2.
[81] Xue K, Sarkar R, Motz C, Asami S, Decker V, Wegner S, et al. Magic-Angle Spinning Frequencies beyond 300 kHz Are Necessary To Yield Maximum Sensitivity in Selectively Methyl Protonated Protein Samples in Solid-State NMR. The Journal of Physical Chemistry C. 2018;122:16437-42.
[82] Asami S, Reif B. Accessing Methyl Groups in Proteins via 1H-detected MAS Solid-state NMR Spectroscopy Employing Random Protonation. Scientific Reports. 2019;9.
[83] Schanda P, Huber M, Boisbouvier J, Meier BH, Ernst M. Solid-state NMR measurements of asymmetric dipolar couplings provide insight into protein side-chain motion. Angew Chem Int Ed Engl. 2011;50:11005-9.
[84] Xue K, Sarkar R, Tosner Z, Lalli D, Motz C, Koch B, et al. MAS dependent sensitivity of different isotopomers in selectively methyl protonated protein samples in solid state NMR. Journal of Biomolecular NMR. 2019;73:625-31.
[85] Barbet-Massin E, Huang C-T, Daebel V, Hsu S-TD, Reif B. Site-Specific Solid-State NMR Studies of “Trigger Factor” in Complex with the Large Ribosomal Subunit 50S. Angewandte Chemie International Edition. 2015;54:4367-9.
[86] Barbet-Massin E, van der Sluis E, Musial J, Beckmann R, Reif B. Reconstitution of Isotopically Labeled Ribosomal Protein L29 in the 50S Large Ribosomal Subunit for Solution-State and Solid-State NMR. Protein Complex Assembly2018. p. 87-100.
[87] Mainz A, Religa TL, Sprangers R, Linser R, Kay LE, Reif B. NMR Spectroscopy of Soluble Protein Complexes at One Mega-Dalton and Beyond. Angewandte Chemie International Edition. 2013;52:8746-51.
[88] Xue K, Sarkar R, Lalli D, Koch B, Pintacuda G, Tosner Z, et al. Impact of Magnetic Field Strength on Resolution and Sensitivity of Proton Resonances in Biological Solids. The Journal of Physical Chemistry C. 2020;124:22631-7.
[89] Chávez M, Wiegand T, Malär AA, Meier BH, Ernst M. Residual dipolar line width in magic-angle spinning proton solid-state NMR. Magnetic Resonance. 2021;2:499-509.

[90] Hassan A, Quinn CM, Struppe J, Sergeyev IV, Zhang C, Guo C, et al. Sensitivity boosts by the CPMAS CryoProbe for challenging biological assemblies. Journal of Magnetic Resonance. 2020;311.
[91] Chen P, Albert BJ, Gao C, Alaniva N, Price LE, Scott FJ, et al. Magic angle spinning spheres. Science Advances. 2018;4.
[92] Gao C, Judge PT, Sesti EL, Price LE, Alaniva N, Saliba EP, et al. Four millimeter spherical rotors spinning at 28 kHz with double-saddle coils for cross polarization NMR. Journal of Magnetic Resonance. 2019;303:1-6.
[93] Bouleau E, Saint-Bonnet P, Mentink-Vigier F, Takahashi H, Jacquot JF, Bardet M, et al. Pushing NMR sensitivity limits using dynamic nuclear polarization with closed-loop cryogenic helium sample spinning. Chemical Science. 2015;6:6806-12.
[94] Callon M, Malär AA, Pfister S, Rímal V, Weber ME, Wiegand T, et al. Biomolecular solid-state NMR spectroscopy at highest field: the gain in resolution at 1200 MHz. 2021.
[95] Nimerovsky E, Movellan KT, Zhang XC, Forster MC, Najbauer E, Xue K, et al. Proton Detected Solid-State NMR of Membrane Proteins at 28 Tesla (1.2 GHz) and 100 kHz Magic-Angle Spinning. Biomolecules. 2021;11.

Glossary of Abbreviations:

ABMS: Anisotropy of the Bulk Magnetic Susceptibility
CP: Cross Polarization
FWHM: Full Width at Half Maximum
HSQC: Heteronuclear Single Quantum Spectroscopy
INEPT: Insensitive Nuclei Enhanced by Polarization Transfer
NMR: Nuclear Magnetic Resonance
MAS: Magic Angle Spinning
RAP: Reduced Adjoining Protonation
SH3: Src-homology 3
SNR: Signal to Noise Ratio